Supporting Information:

Benchmarking the Performance of Lithiated Metal Oxide Interlayers at the LiCoO$_2$|LLZO Interface

André Müller,*,† Faruk Okur,†,‡ Abdessalem Aribia,† Nicolas Osenciat,† Carlos A. F. Vaz,¶ Valerie Siller,§ Mario El Kazzi,§ Evgeniia Gilshtein,† Moritz H. Futscher,† Kostiantyn V. Kravchyk,†,‡ Maksym V. Kovalenko,†,‡ and Yaroslav E. Romanyuk*,†

†*Laboratory for Thin Films and Photovoltaics, Empa - Swiss Federal Laboratories for Materials Science and Technology, Überlandstrasse 129, CH-8600 Dübendorf, Switzerland*

‡*Laboratory of Inorganic Chemistry, Department of Chemistry and Applied Biosciences, ETH Zürich, CH-8093 Zürich, Switzerland*

¶*Swiss Light Source, Paul Scherrer Institut, CH-5232 Villigen PSI, Switzerland*

§*Electrochemistry Laboratory, Paul Scherrer Institut, CH-5232 Villigen PSI, Switzerland*

E-mail: andre.mueller@empa.ch; yaroslav.romanyuk@empa.ch

Phone: +41 58 765 4608; +41 58 765 4169

1   XAS spectra of the interlayers

Figure S1a shows the Co L$_{2,3}$ XAS data for all investigated specimens. As can be seen, there is no noticeable difference between the different interlayers. The only discernible difference is between the as-deposited and co-sintered specimens. The change in peak shape is consistent

with an increase in local order in the cobalt environment.

A similar pattern applies to the O K-edge (Figure S1b). There is again no noticeable difference between different interlayers at the same temperatures. However, while the typical carbonate feature for the as-deposited sample appears only imperceptibly, a clear increase can be seen in the annealed condition overlapping the weaker signals of LCO and LLZO. In view of the fact that all all samples were always handled under inert atmosphere or high vacuum and were not in contact with the environment, we attribute this increase to contamination during sputtering by carbon residues from other processes. Subsequent annealing in a pure oxygen atmosphere eventually leads to oxidation of the carbonates. This is supported by the fact that the pristine LLZO sample, which was not in the sputtering chamber, has no Li_2CO_3 feature.
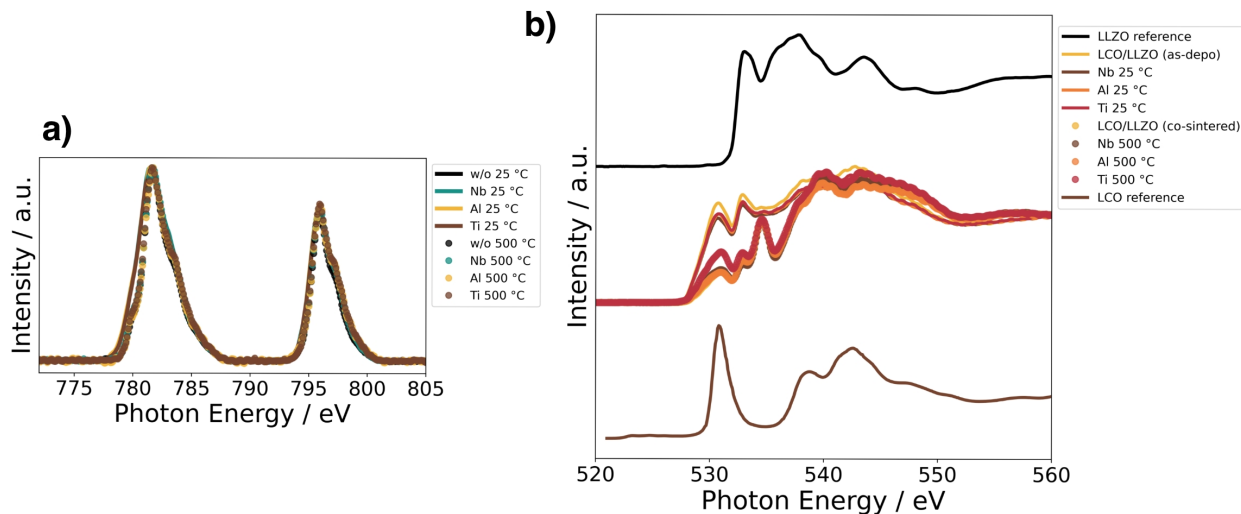

Figure S1: a) Co $L_{2,3}$ X-ray absorption spectroscopy data, and b) O K X-ray absorption spectra in fluorescence mode (TFY) for as-deposited and co-sintered samples at 500 °C in oxygen.

2 EIS deconvolution

To display the deconvolution of the impedance spectra in a more convenient way, the EIS data are shown at various magnifications using Li-Nb-O as an example. The semicircle

in the high-frequency region can be assigned to the LLZO pellet (Figure S2c). Because the measurements were carried out at room temperature, the contributions from grains and from grain boundaries to the LLZO conductivity overlap and cannot be distinguished.

Subsequently, another semicircle in the middle frequency region can be assigned to the cathode-electrolyte interface (int_1) and determines the charge transfer resistance (Figure S2d). Due to the fairly small $semicircle_1$ compared to the $semicircle_2$ of the CC-electrolyte interface (int_2), $semicircle_1$ is not visible (Figure S2e).

We attribute the differences in resistance and capacitance values for int_2 to differences in the surface characteristics, e.g., roughness, which can have a significant influence. The low-frequency tail is due to the blocking effect of the Au electrodes.
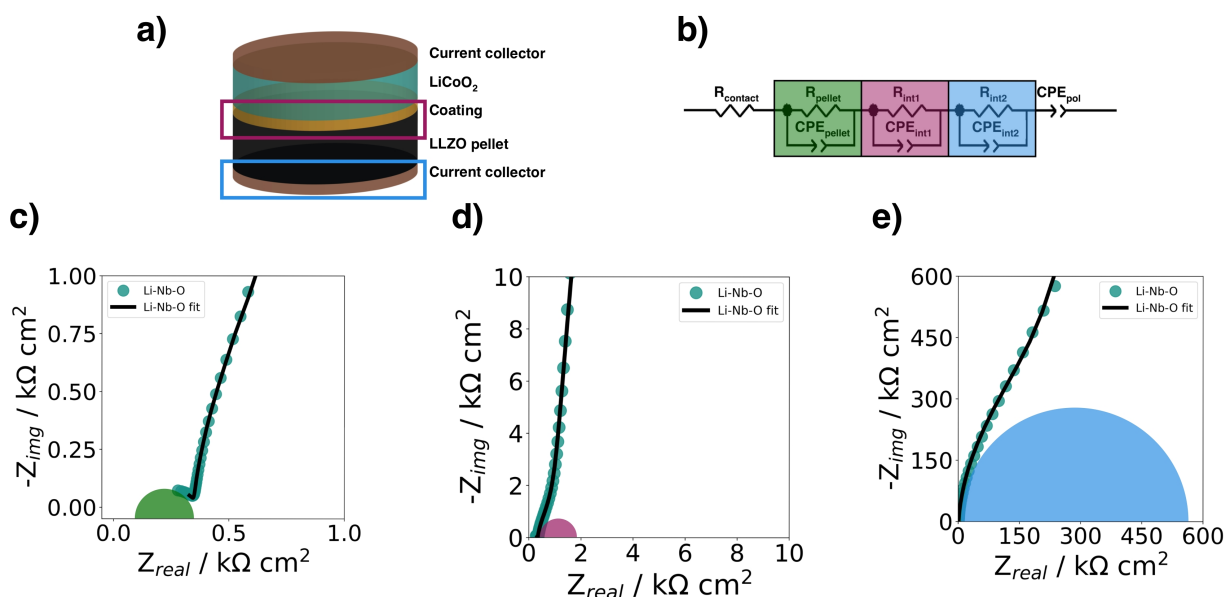

Figure S2: a) Schematic of the half-cell structure for room temperature electrochemical impedance spectroscopy for symmetric cells, b) equivalent circuit for fitting the impedance spectra, and c)-e) deconvolution of the Nyquist plot using Li-Nb-O as an example with different magnifications.

Table S1: Fitted equivalent circuit parameters from the complex impedance spectra for samples with interlayer

Interlayer	$R_{contact}$ (Ω)	R_{pellet} (Ω)	CPE-T_{pellet} (F)	CPE-P_{pellet} (a.u.)	R_{int1} (Ω)	CPE-T_{int1} (F)	CPE-P_{int1} (a.u.)	R_{int2} (Ω)	CPE-T_{int2} (F)	CPE-P_{int2} (a.u.)	CPE-T_{pol} (F)	CPE-P_{pol} (a.u.)
w/o	370.2	124.3	1.77×10^{-9}	0.90	15799	3.40×10^{-8}	1.2	9.04×10^{5}	3.92×10^{-8}	0.87	3.40×10^{-8}	1.15
Li-Nb-O	372	226	4.69×10^{-10}	0.89	1093	1.83×10^{-8}	0.94	5.93×10^{5}	1.77×10^{-8}	0.94	1.64×10^{-8}	0.98
Li-Al-O	370.2	162.9	1.67×10^{-9}	0.88	4098	2.65×10^{-8}	0.98	1.13×10^{6}	3.88×10^{-8}	0.89	3.05×10^{-8}	0.91
Li-Ti-O	410.9	160.6	8.45×10^{-10}	0.93	4817	1.62×10^{-8}	1	332970	1.06×10^{-7}	0.83	6.06×10^{-8}	0.859

Figure S3 shows the EIS data for an LLZO pellet in non-blocking electrode configuration (Li/LLZO/Li) and in blocking electrode configuration (Au/LLZO/Au). The non-blocking measurement was conducted at room temperature from 35 MHz down to 10 Hz. The extracted ionic conductivity was calculated from this data given by:

$$\sigma_{ion} = \frac{l}{R_{total}A},$$

(1)

where R_{total} is the total resistance (bulk + grain) of the electrolyte, l is the sample thickness, and A is the area.
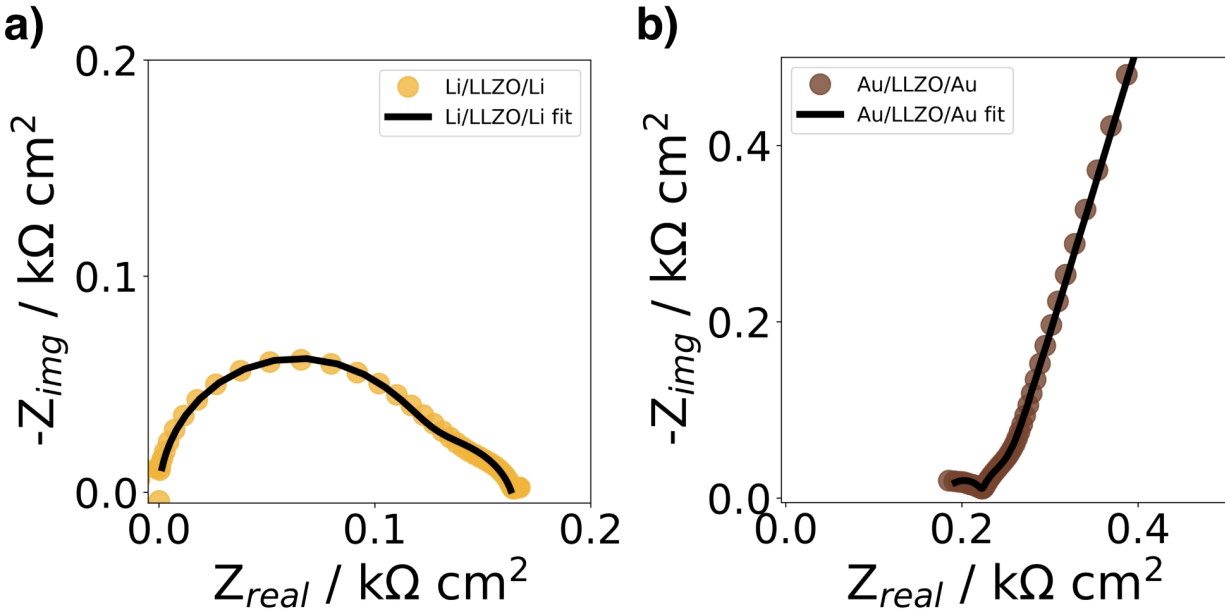

Figure S3: Electrochemical impedance data of a) LLZO pellet in non-blocking electrode configuration (Li/LLZO/Li) , and b) LLZO pellet in blocking electrode configuration (Au/LLZO/Au).

Table S2: Fitted equivalent circuit parameters from the complex impedance spectra for Li/LLZO/Li.

Parameter	Value
R_{bulk} / Ω	945.8
CPE-T$_{bulk}$ / F	3.26 x 10^{-10}
CPE-P$_{bulk}$ / a.u.	0.98371
R_{grain} / Ω	353.7
CPE-T$_{grain}$ / F	1.75 x 10^{-7}
CPE-P$_{grain}$ / a.u.	0.78594

Table S3: Fitted equivalent circuit parameters from the complex impedance spectra for Au/LLZO/Au.

Parameter	Value
$R_{contact}$ / Ω	365.3
R_{pellet} / Ω	80.5
CPE-T_{pellet} / F	4.80×10^{-9}
R_{int1} / Ω	38.2
CPE-T_{int1} / F	5.30×10^{-8}
CPE-P_{int1} / a.u.	1.066
CPE-T_{pol} / F	9.91×10^{-7}
CPE-P_{pol} / a.u.	0.81184

3 Coulombic efficiency

Figure S4 shows the coulomb efficiency of the different cells and shows that it does not approach the desired values of 99.5 %+ achieved in liquid electrolytes. Moreover, there is degradation in each cycle, and none of the coatings significantly improves the efficiency.
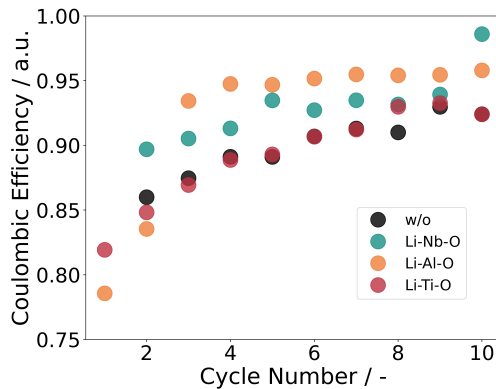

Figure S4: Coulombic efficiency of the different cells.

4 Electrochemical impedance spectroscopy of full cells

Figure S5 shows the impedance spectra for each cell in the pristine state at room temperature, before the start of the CV measurement at 80 ℃, and after the CV scans at 80 ℃. The impedance increases after the CV scan for the w/o, Li-Al-O and Li-Ti-O interlayers. For the

Li-Nb-O cell, the impedance decreases with cycling, which is in contrast to the other cells. The decrease could be related to voltage drop of the Li-Nb-O cell.
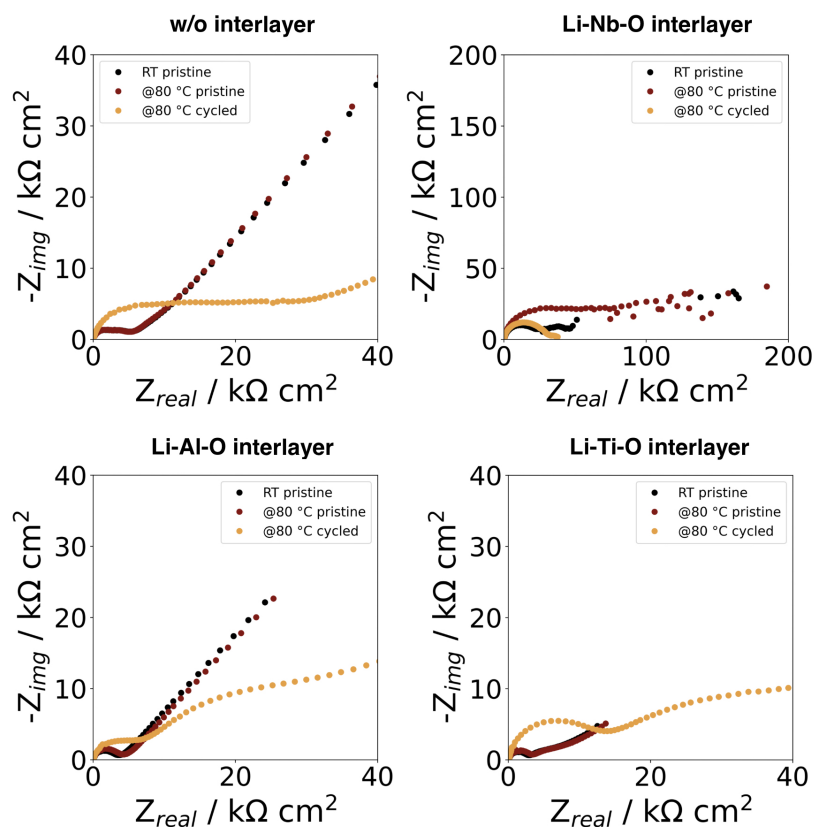

Figure S5: Electrochemical impedance spectra of the cycled full cells for each interayer.

5   Voltage drop around 3.9 V

The unexplained voltage drop in the Li-Nb-O case remains very intriguing. This feature is consistent with CV scans and galvanostatic charge/discharge experiments of the Li-Nb-O interlayer shown. Similar voltage drops were also observed in samples without an interlayer (Figure S6). For demonstration purposes, only cycles 1, 2, 6, and 9 are shown. However, the feature can be found in all cycles. There is no plausible explanation yet. However, we are currently investigating the cause in more detail. Similar voltage drops in the discharge process between 3.9 and 3.8 V are reported by Liu et al.[60] and Luo et al.[61].
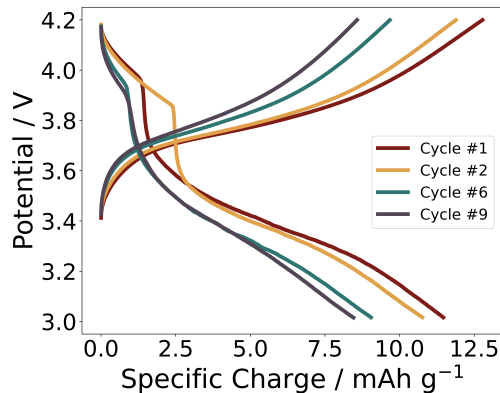
Figure S6: Exemplaric charge–discharge curves for a full cell without interlayer for the cycles 1, 2, 6, and 9. The voltage drop could be seen in all cycles.

6 GI-XRD

The X-ray diffraction patterns of LLZO and LCO have comparable peaks, making it difficult to distinguish between the two. To address this, we performed GI-XRD analysis with an incident angle of 1.5° in the 42° - 47° range on a cell with Au/LCO/LLZO structure. Our results showed that our LCO does not have a clear peak in this region but rather a shoulder around 45.3°. Our analysis suggests that the Au top layer is possibly masking the XRD pattern, leading to the reduced intensity and limited visibility of the peaks. Specifically, it appears that the presence of the Au layer causes the XRD pattern of LCO to be attenuated, resulting in the observed shoulder-like feature around 45.3°.
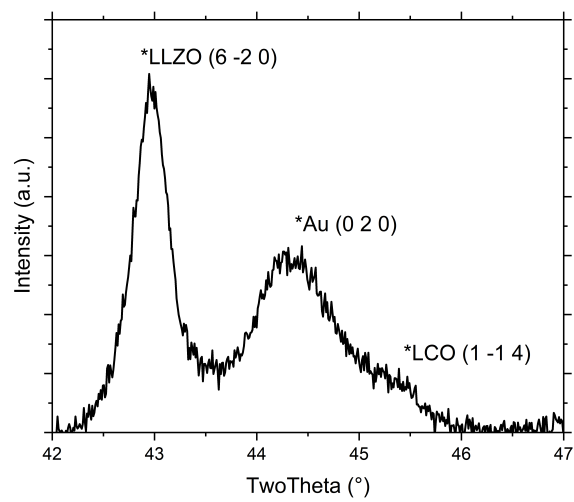
Figure S7: GI-XRD analysis of AU/LCO/LLZO stack